Hydrogels with Controlled, Surface Erosion Characteristics from Self-Assembly of Fluoroalkyl-Ended Poly(ethylene glycol)

Giyoong Tae,[†] Julia A. Kornfield,*[,†] Jeffrey A. Hubbell,[‡] Diethelm Johannsmann,[§] and Thieo E. Hogen-Esch[||]

Division of Chemistry and Chemical Engineering, 210-41 California Institute of Technology, Pasadena, California 91125, Institute for Biomedical Engineering and Department of Materials, ETH-Zurich and University of Zurich, 8044 Zurich, Switzerland, Max Planck Institute fur Polymerforschung, Postfach 3148, 55021 Mainz, Germany, and Loker Hydrocarbon Research Institute, University of Southern California, Los Angeles, California 90089

Received May 1, 2001

ABSTRACT: Poly(ethylene glycol) (PEG) (M_w = 6k, 10k, and 20k g/mol) terminated at both ends by hydrophobic fluoroalkyl segments ($-(CH_2)_2C_nF_{2n+1}$, n = 6, 8, or 10) was synthesized and demonstrated to self-assemble into hydrogels with phase behavior and mechanical and erosion properties that can be systematically varied by molecular design. With increasing fluoroalkyl length relative to PEG length, the phase behavior of these polymers in aqueous solution changes from the single-phase behavior of familiar associative thickeners, to sol−gel coexistence, to precipitation. For those polymers that exhibit sol−gel coexistence, the equilibrium gel concentration (or swelling ratio of the gel phase) and the modulus of the gel phase are governed by the length of the PEG midblock, whereas the relaxation time is determined by the hydrophobe length. The erosion characteristics of these hydrogels correlate with their phase behavior. The gels of sol−gel coexisting species exhibit surface erosion in an open system with a slow dissolution rate controlled by the end-group length; in contrast, hydrogels from polymers that show single-phase behavior exhibit bulk erosion that is relatively fast. Therefore, the molecular structure of this class of polymers produces hydrogels whose mechanical and erosion properties can be tailored for desired applications. Based on the established biocompatibility of PEG, the degree to which the characteristics of the gel phases can be tailored, and the surface erosion characteristics that can be achieved, these materials might have applications in implantable drug-release depots.

Introduction

Bioerodible and biocompatible polymers are widely used in medicine for drug delivery and medical devices.[1] Relatively hydrophobic biodegradable polymers, e.g., poly(α-hydroxyl esters),[1−3] polyortho esters,[4] and polyanhydrides,[5] have been successfully developed and used for the controlled release of hydrophobic drugs and as materials in structural supports such as surgical sutures, staples, and meshes. However, there also exists a need for hydrophilic resorbable materials that can incorporate protein drugs or cells[6] or be used to guide wound healing, e.g., to prevent postoperative adhesion formation.[7] Degradable hydrogel systems have been studied for such purposes because of their inherent hydrophilicity and biocompatibility.[8]

The application of natural hydrogels, such as gelatin, collagen, or polysaccharides, has the advantage of exploiting preexisting and sometimes evolutionarily developed biological interactions and degradation pathways but is limited by the difficulty of tailoring the degradation rate, as well as by uncertain immunological responses and potentially difficult isolation and purification procedures.[1,6] The majority of synthetic biodegradable hydrogels are based on poly(ethylene glycol) (PEG) because of its favorable properties of biocompatibility, nontoxicity, and nonimmunogenicity.[9]

* Correspondence to Prof. Julia A. Kornfield, Division of Chemistry and Chemical Engineering 210-41, California Institute of Technology, Pasadena, CA 91125. Tel.: 626 395 4138. Fax: 626 568 8743. E-mail: jak@cheme.caltech.edu.
[†] California Institute of Technology.
[‡] ETH-Zurich and University of Zurich.
[§] Max Planck Institute fur Polymerforschung.
[||] University of Southern California.

Most PEG-based degradable hydrogel systems developed so far have been made by incorporating a variety of cross-linkers to create a gel network and degradation sites to induce degradation in the biological environment. In most cases, hydrolytically labile sites such as esters have been incorporated;[6,7,10] alternatively, enzymatic degradation sites have been introduced to achieve a degradative response to biological stimuli.[11]

PEGs modified with hydrophobes at both ends have been investigated widely as model associative polymers.[12−26] These physically cross-linked systems have potential applications as thickeners, adhesives, adsorbents, coatings, flocculants for wastewater treatment, surfactants and stabilizers for heterogeneous polymerization,[12] and DNA separating sequencing media.[14,15] The majority of the systems studied so far do not exhibit phase separation, but rather form a single phase over the entire concentration range.[13−15,22−26] As the concentration of polymer dissolved in water increases, the size of the connected clusters of associative polymers grows continuously and finally forms an infinite gel-like cluster. This can be regarded as a sol−gel transition, but is not a thermodynamic phase transition.[12] Above a critical concentration at which the viscosity starts to increase rapidly, all properties of systems existing as a single phase change in a continuous manner with concentration. The rheology of single-phase systems has been modeled in terms of the concentration-dependent topology of aggregation and by breakage of the junction between micelles (bridging chains).[13]

Recently, phase separation has been reported for PEGs modified with long alkyl groups. Francois et al. observed that systems of 2000-g/mol (2-kD) and 4-kD

10.1021/ma0107511 CCC: $20.00
Published on Web 07/31/2001

PEG modified with $-C_{12}H_{25}$ hydrophobes and 20-kD PEG modified with $-C_{18}H_{37}$ form quasi-elastic gels at high concentration,[19] and Pham et al. reported that aqueous solutions of 35-kD PEG with C18 alkyl groups or PEGs from 20 to 35 kD with C16 alkyl groups separate into a highly viscous lower phase and a low-viscosity upper phase.[16−18] Unlike the general phase diagram of physical gel systems showing an upper critical solution temperature (UCST),[27] the equilibrium concentrations of sol and gel of the hydrophobically modified PEGs are either temperature-insensitive,[17] or the equilibrium gel-phase concentration increases weakly with increasing temperature (LCST behavior was even found in some cases).[19] Temperature-insensitive phase behavior can be explained in terms of an entropically driven association process,[17] and an increase in equilibrium gel concentration or LCST behavior can be explained by the poorer solvation of PEG chains with increasing temperature.[19]

Semenov et al. provided the first theoretical prediction of phase separation of telechelic associative polymer solutions in the limit of high aggregation number.[28] The phase behavior is governed by the competition between osmotic repulsion among micelles composed of the telechelic polymers (analogous to star polymers and diblock micelles) and attraction resulting from the increase in configurational entropy of the system when bridges form between micelles. The entropic attraction increases with aggregation number. When the attraction is sufficiently large to overcome the repulsion, the system separates into two phases: a close-packed "solid" phase of micelles and a dilute "gas" phase of micelles and free chains. Recently, Pham et al. advanced an alternative view in which the phase separation is viewed as a coexistence of a liquid and a gas of micelles.[17] By modeling the associative micelles as adhesive hard spheres, they were able to capture sol−gel coexistence and to qualitatively describe the sol and gel compositions. Thus, this approach has the potential of offering more quantitative predictions than the purely scaling approach of Semenov. However, the discrepancy between the semiempirically inferred value of the "stickiness parameter" and the theoretical value expected for the observed aggregation number was large (3 orders of magnitude). This difficulty is likely to be related to the function describing the intermicelle interaction potential.

Here, we explore hydrogels made from the self-assembly of PEG molecules modified at both ends with fluoroalkyl end groups (R_f-PEGs) that are sufficiently long to exhibit sol−gel coexistence, particularly examining their potential as degradable carriers that have controlled rheological properties and erosion rates. Through the maintenance of the benefits of PEG-based hydrogels and the use of physical junctions between chemically inert fluoroalkyl groups, these materials have been designed with biocompatibility in mind. The physical nature of the junction provides a route to surface erosion of the hydrogels when exposed to an open environment, in contrast to strategies that incorporate degradation sites. Thus, the gel maintains the modulus of the equilibrium composition and erodes in a predictable manner via desorption of chains and micelles, followed by their diffusion into the reservoir. In addition, moving into the sol−gel coexistence regime by using strong hydrophobic end groups avoids the rapid bulk erosion characteristic of single-phase systems.

Table 1. Bifunctional R_f-PEGs

sample	PEG block (kg/mol)	end group[a]	conversion[b] (%)
20KC8	20	$-C_8F_{17}$	96
20KC10		$-C_{10}F_{21}$	97 (92)
10KC8	10	$-C_8F_{17}$	94
10KC10		$-C_{10}F_{21}$	94 (96)
6KC6	6	$-C_6F_{13}$	99
6KC8		$-C_8F_{17}$	89
6KC10		$-C_{10}F_{21}$	97 (97)

[a] Full end group is $-$IPDU$-(CH_2)_2-C_nF_{2n+1}$, where IPDU is

[b] Degree of substitution as determined by ^{19}F NMR spectroscopy (selected values determined by HPLC are in parentheses).

We describe the phase behavior, mechanical properties, and erosion characteristics of a range of materials, including polymers that exhibit sol−gel coexistence. By spanning a wide range of PEG and fluoroalkyl lengths, the results enable the molecular design of materials that have desired phase behavior (single-phase vs sol−gel coexistence) with systematically varied mechanical and erosion properties.

Experimental Section

Synthesis of End-Group-Modified PEGs. Poly(ethylene glycol) (PEG) (with alcohol functionalities at both ends) of nominal molecular weights 6000 g/mol (6 kD) (from Fluka, Milwaukee, WI), 10 kD (from Aldrich, Milwaukee, WI), and 20 kD (from Fluka) were used to prepare telechelic R_f-PEGs. Monomethoxy PEGs (i.e., with a methyl terminating group on one end and alcohol on the other) of nominal molecular weights 2 and 5 kD (from Aldrich) were used to prepare monofunctional R_f-PEGs. Three different fluorinated alcohols ($C_nF_{2n+1}CH_2CH_2$-OH, n = 6, 8, 10) were purchased from Lancaster Synthesis Inc. (Windham, NH). Isophorone diisocyanate (IPDI), dibutyltin diacetate, and anhydrous tetrahydrofuran (THF) were purchased from Aldrich. Anhydrous ethyl ether was from EM Science (Hawthorne, NY).

The method of Glass et al.[25] was used to attach fluorinated end groups to the terminal hydroxyls of the polymers. The PEG was dried by azeotropic distillation in toluene and was reacted with a 100-fold molar excess (with respect to end groups) of vacuum-distilled IPDI in anhydrous THF for 48 h. This isocyanate-functionalized intermediate was precipitated in anhydrous ethyl ether to remove unreacted IPDI and was subsequently reacted with a 10-fold excess of fluorinated alcohol in anhydrous THF for 48 h with the addition of dibutyltin diacetate. The reaction mixture was precipitated in anhydrous ethyl ether, dissolved in THF, and reprecipitated. All reactions were done under argon.

The degree of substitution of the PEG termini with R_f groups was determined by ^{19}F NMR spectroscopy using CF_3COOH or CF_3SO_3Na ($\delta \approx -78$ ppm) as an internal standard and measuring the ratio of the peak intensites of the sample (CF_3^-, $\delta \approx -83$ ppm) and of the standard, according to the method of Zhang et al.[29] The samples prepared for this study are described in Table 1, where the abbreviation *n*KC*m* denotes a polymer with a PEG midblock of MW *n* kg/mol and *m*-carbon fluoroalkyl end groups, i.e., $C_mF_{2m+1}CH_2CH_2-$PEG$-CH_2CH_2-C_mF_{2m+1}$. To verify the degree of conversion of the ends as determined by ^{19}F NMR spectroscopy, each sample modified with $-C_{10}F_{21}$ was also characterized using reverse-phase HPLC. A C18 column was used with a Waters HPLC system and eluted using a gradient input of mixed solvent (from 20/80 acetonitrile/water to 100% acetonitrile), which can separate unmodified, one-end-modified, and two-end-modified PEG. Good agreement between the values obtained by HPLC (shown in parentheses in Table 1) and the values obtained by ^{19}F NMR spectroscopy support the reliability of the NMR method.

Monofunctional R_f-PEGs were also prepared similarly using monomethoxy PEGs of nominal molecular weights 2 and 5 kD.

Characterization of Sol−Gel Equilibria. In a vial, weighed amounts of fine particles of dried bifunctional R_f-PEGs were dissolved in deionized water, and the mixtures were mechanically shaken for 24 h. Experiments were performed at a number of concentrations, 1 wt % and greater. For samples that demonstrated phase separation, the gel phase in contact with the dilute phase formed at the bottom of the vial because of the slightly higher density of PEG and fluoroalkyl groups than water.

Gel-phase concentrations were obtained by measuring wet and dry weight as follows. After decanting off the dilute phase, the gel phase was weighed; then the gel phase was vacuum-dried and weighed again. The ratio of the two weights was regarded as the concentration of the gel phase.

Concentrations of the dilute sol phase in equilibrium with the gel phase ($C_{sol,eq}$) were measured using complex formation of PEG with barium and iodine.[30] To 2 mL of sample solution was added 0.5 mL of a 5% (w/v) solution of $BaCl_2$ in 1 N HCl. Then, 0.25 mL of standard 0.1 N iodide solution (Aldrich) was added. Ten minutes after addition of the I_2 solution, the absorbance at 535 nm was measured. A standard calibration line was obtained using 1, 5, 10, and 25 μg/mL solutions of PEG; the plot displayed a linear relationship between PEG concentration and absorbance ($r^2 = 0.9973$). To remove any unwanted dispersed gel phase in the sol phase, the dilute phase was removed and centrifuged, and then the supernatant was used. The supernatant was diluted to the appropriate range of concentration for this analytical method.

Mechanical Property Measurements. Samples were prepared as described above. The mixing time was adjusted to achieve an apparent equilibrium, as determined by the disappearance of light scattering from the sample. The prepared samples were centrifuged before being loaded to remove any entrapped bubbles. A stress-controlled rheometer (SR 5000, Rheometric Scientific, Piscataway, NJ) equipped with a solvent trap was used with a cone-and-plate geometry (0.1-rad cone angle and 25-mm diameter) to obtain the rheological data. With the appropriate solvent trap, drying of the sample was negligible for 12 h at 25 °C.

Characterization of Erosion of Gel Phases. Erosion of the gel phase was observed using surface plasmon resonance (SPR).[31] The surface plasmon resonance angle of a thin gold film is sensitive to the thickness and refractive index of a layer polymer gel in contact with it. On one side of a glass slide, a gold film (~50 Å) was deposited, and polymers were spin-coated onto the gold surface from solution in ethanol. The thickness of the coated film was measured using a profilometer (α-stepper). A 10% solution of polymer in ethanol was spun at 2000 rpm to give a film of ~1-μm thickness; the thickness was increased or decreased by varying the concentration of the polymer solution. The polymer-coated gold slide was assembled into the optical apparatus so that the glass side was facing the prism and the polymer-coated side was exposed to a flowing stream of deionized water at 25 °C (Figure 1a). The change in resonance angle was recorded as a function of time. The changes in resonance angle reflect changes in film thickness and refractive index that occur during initial swelling and subsequent erosion of the polymer layer (Figure 1b). This technique works well for relatively slow erosion rates (so that a thin film of a few microns thickness erodes over several hours or more). For faster erosion rates, a simple experiment on very thick samples (~1 cm) placed in a vial with an excess of water was used that involved simple detection of the dissolved amount in the supernatant, which was refreshed at regular intervals.

Results

Phase Behavior. The phase behavior of bifunctional R_f-PEGs is governed by the relative length of the PEG chain and the fluoroalkyl end groups (Table 3). Increasing the PEG length increases the solubility of the polymer in water, whereas increasing the length of the hydrophobe decreases the solubility. For a given length of PEG, if the hydrophobe is too short, no phase separation occurs; the polymer simply dissolves into a single phase. For example, 20KC10 and 20KC8 exist as homogeneous solutions over the whole range of concentrations, although the viscosity increases dramatically as the concentration of polymer increases. On the other hand, if the hydrophobe is too long, it might not be possible to dissolve the polymer at all (e.g., 6KC10). Thus, for 6-kD PEG, a C10 fluorocarbon hydrophobe is too long to exist as a sol phase; for 10-kD PEG, both hydrophobes examined, C8 and C10, are in the right range to produce sol−gel phase separation; and for 20-kD PEG, even a C10 fluorocarbon hydrophobe is too short to cause sol−gel phase separation.

For polymers that exhibit sol−gel coexistence, the degree of swelling (the inverse of the concentration of the gel phase) in the equilibrium gel is controlled mainly by the PEG length (Table 3). When the PEG length is fixed and the hydrophobe length is varied, the swelling ratio is nearly constant (cf. 10KC10 to 10KC8 and 6KC8 to 6KC6). The swelling ratio increases with increasing PEG length (cf. 6KC8 to 10KC8), which is analogous to reducing cross-link density.

The phase boundary is insensitive to temperature: increasing the temperature (up to 80 °C) does not lead

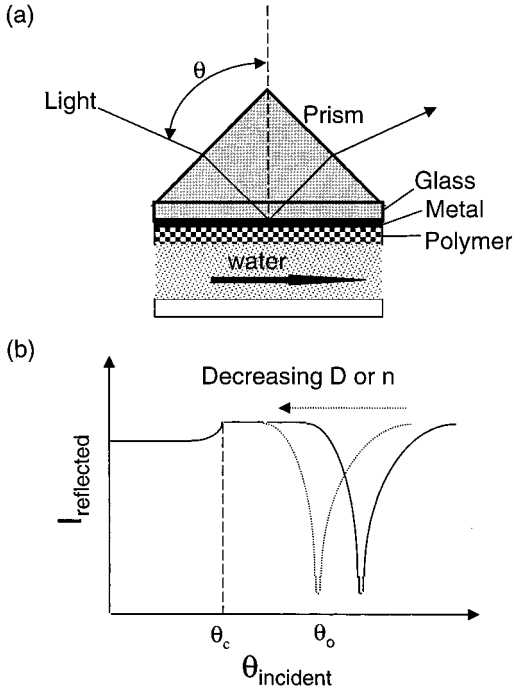

Figure 1. Schematic diagram of the surface plasmon resonance (SPR) experiment in contact with a flowing system: (a) sample configuration, (b) qualitative behavior of the resonance angle θ_o with decrease in the thickness D or refractive index n of the polymer layer adjacent to the metal film.

Table 2. Monofunctional R_f-PEGs

sample	PEG block (kg/mol)	end group[a]	conversion[b] (%)
5K-M-C10	5 kg/mol	$-C_{10}F_{21}$	91%
5K-M-C8		$-C_8F_{17}$	91
2K-M-C10	2	$-C_{10}F_{21}$	89

[a] Full end group is $-$IPDU$-(CH_2)_2-C_nF_{2n+1}$, where IPDU is

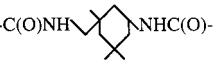

[b] Degree of substitution as determined by ^{19}F NMR spectroscopy.

Table 3. Phase Behavior of Bifunctional R_f-PEGs at 25 °C

sample	type of phase behavior	equilibrium compositions in water (wt %)		equilibrium compositions in PBS (wt %)	
		$C_{gel,eq}$[a]	$C_{sol,eq}$[b]	$C_{gel,eq}$	$C_{sol,eq}$
20KC8	one-phase	N/A	N/A	N/A	N/A
20K10	one-phase	N/A	N/A	N/A	N/A
10KC8	two-phase	6.5 ± 0.2	0.075 ± 0.005	7.8 ± 0.2	0.055 ± 0.002
10K10	two-phase	6.8 ± 0.7	0.019 ± 0.008	8.1 ± 0.7	0.011 ± 0.003
6KC6	two-phase	9.5 ± 0.5	0.066 ± 0.007	10.5 ± 0.6	0.038 ± 0.002
6KC8	two-phase	11.0 ± 0.3	0.042 ± 0.007	12.5 ± 0.3	0.017 ± 0.001
6KC10	insoluble	N/A	N/A	N/A	N/A

[a] Equilibrium gel-phase concentration. [b] Equilibrium sol-phase concentration.

to any noticeable change of the gel-phase concentration for the sol−gel coexisting systems. This insensitivity to temperature is in accord with previously reported hydrocarbon-ended phase-separating systems, as well as with theoretical descriptions[17] in terms of the entropically driven formation of a concentrated phase. The tradeoff between the entropy associated with the center-of-mass positional freedom in the micelle gas and the configurational entropy of the end groups distributing among multiple micelle cores in the dense phase governs the phase behavior, so the temperature dependence cancels out.

A comparison of the behavior in deionized water with that in phosphate-buffered saline (PBS) shows that the gel concentration is slightly higher in PBS than in water and that the sol concentration is consistently lower in PBS than in water (Table 3). This difference is due to the decreased solvation of PEG chains resulting from the salting out effect[32] and the increased aggregation tendency of fluorocarbon end groups because of the added salts in PBS.[29]

The concentrations of the sol phases are very small for all samples (<0.1 wt %), and unlike the gel composition, both the end-group length and the PEG length affect the equilibrium sol concentration (Table 3).

Mechanical Properties of Gel Phases of Sol−Gel Coexising Species at $C_{gel,eq}$. The rheological properties of the gels at their equilibrium compositions show single-relaxation behavior (Figure 2), similarly to previously examined modified PEG systems.[13−15,18,20−22] The dynamic modulus of 10KC10 at $C_{gel,eq}$ shows a very flat plateau in the storage modulus above the frequency of the maximum G'' and its loss modulus drops as ω^{-1} with increasing frequency in the same region. Below ω_x, terminal behavior holds ($G' \sim \omega^2$, $G'' \sim \omega$). These features are characteristics of a single-relaxation-time (or Maxwell) fluid. For a Maxwell fluid, the following relationship holds

$$G''(\omega) = [G'(\omega)G_o - G'(\omega)^2]^{-1/2}$$

where G_o is the plateau modulus. The Cole−Cole plot (G'' versus G') shows a nearly semicircle shape for 10KC10, indicating single-relaxation behavior (Figure 2). Over the accessible range of frequency, 10KC8 and 6KC8 at their respective $C_{gel,eq}$ values appear to behave like 10KC10.[12] As one would expect, 6KC6 has a substantially faster relaxation time, so that, in the frequency range measured (100 rad/s), only terminal-regime behavior is observed.

For gels at their equilibrium compositions, the PEG midblock determines the modulus of the gel phase; similar values in the plateau modulus are observed for 10KC10 and 10KC8 (Figure 3), reflecting the similar densities of physical junctions in these gels, also evident from the similar values of their swelling ratios (Table 3). A higher value was observed for 6KC8, indicating that a higher density of physical junctions is present, which also agrees with its smaller swelling ratio relative to those of 10KC10 and 10KC8.

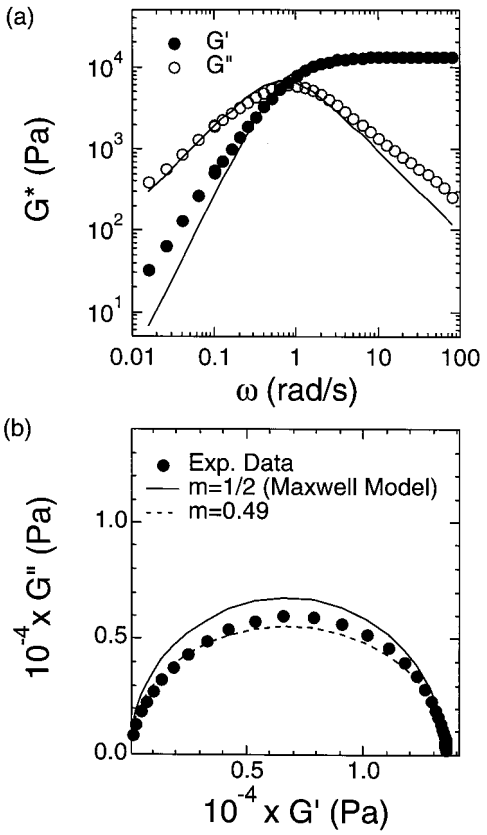

Figure 2. Systems that exhibit sol−gel coexistence show nearly single-relaxation behavior of the equilibrium gel (i.e., at concentration $C_{gel,eq}$), illustrated here by 10KC10: (a) dynamic moduli, (b) Cole−Cole plot. The solid curve is for a single Maxwell element. The dashed curve is for $G''(\omega) = [G'(\omega)G_o - G'(\omega)^2]^{-m}$ with $m = 0.49$. ($T = 25$ °C.)

The viscoelastic relaxation time (τ_r) of these gels, the inverse of the frequency at the loss maximum (ω_x^{-1}) (Figure 3b), increases strongly with the hydrophobe length; the ∼40-fold difference in τ_r between 10KC10 and 10KC8 (Table 4) shows that two CF_2 units significantly increase the average residence time of a given R_f group in a physical junction of the gel (which controls the longest relaxation time).[13−15,18,20−22] Interestingly, 10KC8 and 6KC8 gels in their respective equilibrium states demonstrate similar relaxation times, which indicates that the end group dominates the relaxation behavior. This is in contrast to single-phase-type sys-

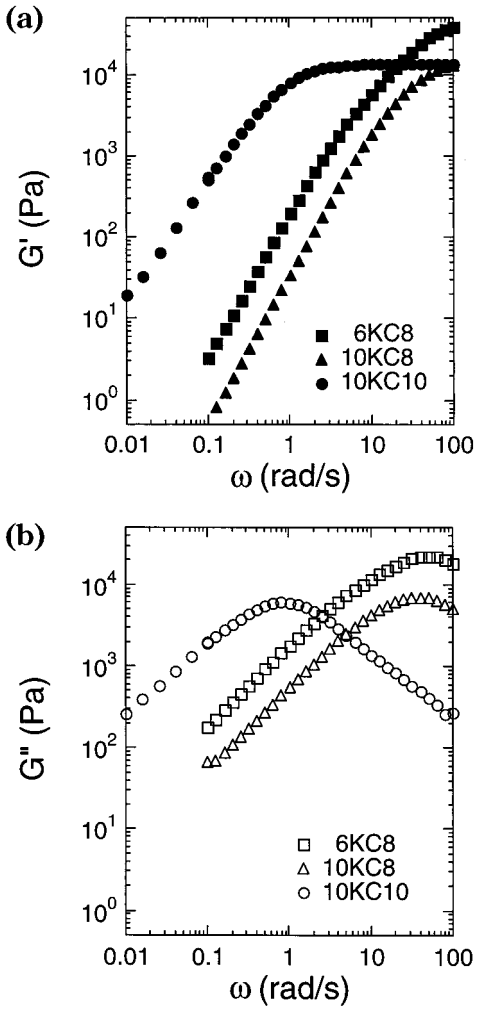

Figure 3. Dynamic moduli of gel phases of sol−gel coexisting species at equilibrium compositions ($C_{gel,eq}$): (a) storage moduli, (b) loss moduli. (T = 25 °C.)

Table 4. Mechanical Properties of Gel Phases at $C_{gel,eq}$ at 25 °C

	10KC10	10KC8	6KC8
composition (%)	6.8	6.5	11.0
relaxation time (τ_r) (s)	1.2	0.029	0.023
plateau modulus (G_o) (kPa)	14.4	18.5	56.1
viscosity (η_o) (kPa s)	18	0.53	1.5

tems, which show strong concentration dependence of τ_r until the concentration is sufficiently large that the bridge/loop ratio is $O(1)$.[13] This insensitivity to concentration (comparing τ_r for 10KC8 and 6KC8) is a consequence of the fact that the equilibrium gel concentrations are high enough that the bridge/loop ratios are already $O(1)$. Finally, the zero-shear viscosity (η_0), which is the product of the plateau modulus and the relaxation time, varies over 1 order of magnitude with modest changes in molecular structure (10KC10 > 6KC8 > 10KC8, Table 4).

Erosion Characteristics. The erosion characteristics of the hydrogels were determined using surface plasmon resonance (SPR). For the hydrogels that exhibit sol−gel coexistence, the transient resonance angle (θ) shows four distinct stages (Figure 4): an initial rapid decrease (τ_0), a small gradual increase to an equilibrium value (τ_1), a constant value for a prolonged period (τ_2), and finally a decrease to the value corresponding to the bare gold surface in contact with water (τ_3). The initial

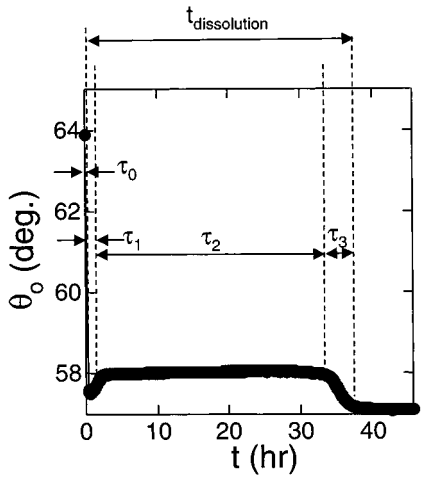

Figure 4. Change of surface plasmon resonance angle with time for 10KC8 film of initial dry film thickness 0.55 μm.

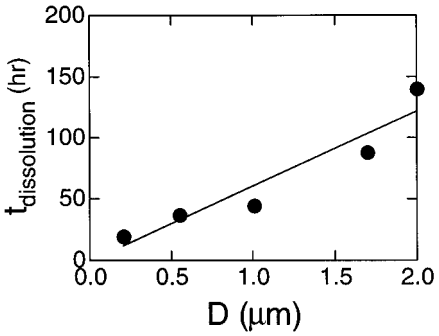

Figure 5. Dissolution time as a function of the initial dry thickness of 10KC8 gels.

rapid decrease of θ during τ_0 is due to swelling from the dried state, which reduces the polymer concentration, producing a concomitant decrease in the refractive index. The resonance angle drops even lower than that of the equilibrium state, θ_{eq}; during the interval τ_1, the resonance angle approaches the equilibrium value. Because the resonance angle tracks the polymer concentration, the fact the θ passes through a minimum in the first ~1 μm adjacent to the gold film indicates that the concentration drops below the equilibrium gel concentration and then rises back to $C_{gel,eq}$. This anomalous overswelling is reminiscent of similar phenomena in a variety of systems.[34] Because the thickness of the swollen film (~8 μm in the example shown in Figure 4) is much greater than the depth probed by SPR (~1 μm), the constant resonance angle observed during τ_2 indicates that the polymer concentration in the gel is constant. The decrease of θ during τ_3 results from the decrease in thickness as the last ~1 μm of the gel erodes.

For a given polymer (10KC8), the resonance angle during the interval τ_2 is independent of the initial thickness of the film, consistent with the polymer concentration being equal to that of the equilibrium gel throughout the periods τ_2 and τ_3. The duration of the prolonged plateau, τ_2, increases linearly with film thickness, consistent with surface erosion of the equilibrium gel at a constant erosion rate. The increase in τ_2 dominates the behavior of the total dissolution time, defined in Figure 4, leading to a linear increase in $t_{dissolution}$ with film thickness (Figure 5). The initial swelling transient (τ_0 and τ_1) is also sensitive to film thickness: As the initial dry thickness increases from

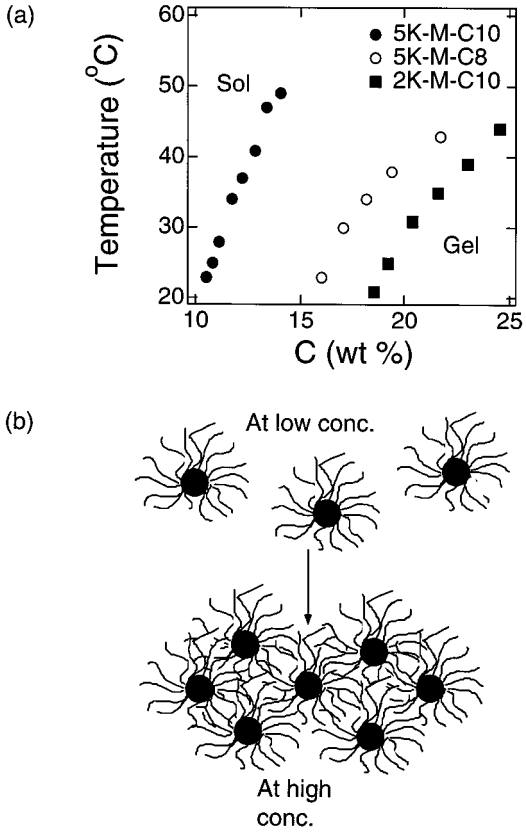

Figure 6. Lyotropic phase transition of one-end-modified PEG solutions: (a) phase diagram, (b) schematic representation.

0.5 to 2 μm, the time for the initial swelling step τ_0 increases from ~0.5 to ~2.5 h, and the depth of the undershoot decreases (for the thickest films studied, the τ_1 interval is no longer well-defined, so the trends in τ_1 with film thickness are not as pronounced). The final transient in $\theta(t)$ during the τ_3 is period is independent of the initial thickness, consistent with the interpretation that this final process occurs at the intrinsic erosion rate for the equilibrium gel of a given polymer as the film decreases in thickness from the threshold of sensitivity of SPR to zero thickness.

The dissolution rate of the polymers that exhibit sol−gel coexistence is computed from the linear relationship between the dry thickness and the dissolution time (e.g., Figure 5). For these species, the dissolution rate appears to be controlled mainly by the hydrophobe length: The dissolution rate of 6KC8 is of the same order of magnitude as that of 10KC8, whereas 10KC10 dissolves at least 100 times slower than 10KC8 (the final stage was too slow to be observed within the experimental time).

For comparison, we also examined the dissolution of two types of hydrogels that do not show sol−gel coexistence: an associative polymer that exhibits the usual single-phase behavior (20KC10) and hydrogels formed by lyotropic ordering of micelles[35] (5KmPC10, Figure 6). In these systems, there is no thermodynamic barrier for dissolution from the bulk, and the driving force for dissolution is the concentration of the polymer matrix (~10^1 wt %), which is much greater than the driving force for dissolution of equilibrium gels (the equilibrium sol concentration for the sol−gel coexisting polymers is only ~10^{-2} wt %). Consistent with the high driving force for dissolution and the continuous change in concentration upon exposure to an open system, the resonance angles of 20KC10 films of initial thicknesses in the range 0.1−2 μm decrease rapidly to their final values without any plateau, which implies fast and homogeneous erosion of the gels. Because the erosion rate was too fast to quantify by SPR, the erosion rates were instead obtained during the initial linear regime of dissolution of thick gels prepared in vials. As expected, 20KC10 and 5KmPC10 exhibit much faster dissolution rates than species that exhibit sol−gel coexistence (~10^2 times faster than the dissolution of 10KC8). The erosion rates of the various samples span 5 orders of magnitude (Table 5).

Table 5. Dissolution Rates at 25 °C[a]

species conc (wt %)	10KC10 (6.8)	10KC8 (6.5)	6KC8 (11.0)	20KC10 (10.0)	5K-M-C10 (12.8)
dissolution rate (mg cm^{-2} h^{-1})	$\ll 10^{-5}$	1.67×10^{-3}	3.33×10^{-4}	0.168	0.201

[a] Note: For systems exhibiting sol−gel coexistence, the compositions of the polymer matrices used are the equilibrium gel concentrations. For single-phase (20KC10) and lyotropic (5K-M-C10) systems, the initial concentrations were chosen to be high enough that gels formed (Figure 6a). For these fast-dissolving gels, the rates are for the initial linear stage of dissolution from the bulk gel state.

The erosion kinetics of the systems with C8 fluoroalkyls roughly track their equilibrium sol concentrations; however, it is interesting to note that the relative erosion rate of 10KC10 is much slower than one would expect on the basis of its equilibrium sol concentration. The usual expectation for surface erosion is that it is limited by the mass transfer rate at the surface, often described in terms of a mass transfer coefficient (mostly determined by the flow conditions at the surface) and the equilibrium concentration of the eroding species. In this series of experiments, the flow conditions are held fixed, and the molecular or micellar diffusivities are similar across all systems. Therefore, the mass transfer coefficient can be regarded as constant, and the ratio of the erosion rates is expected to follow the ratio of the equilibrium sol concentrations. This appears to be a good approximation for 10KC8 and 6KC8, within the uncertainty in determining $C_{sol,eq}$. However, the very large difference in the dissolution rates between 10KC10 and 10KC8 cannot be understood in terms of the small difference (~4 times) in their equilibrium sol concentrations. This suggests that a different physical mechanism applies.

If the rate of diffusion of micelles away from the surface exceeded the rate of release of micelles from the surface, the surface concentration could drop below $C_{sol,eq}$. The overall flux would then be determined by the rate of detachment of micelles from the gel. Our rheological data suggest that this could explain the more than 2 orders of magnitude slower erosion rate for C10 systems than for C8 systems: The rheological relaxation time is approximately 40 times slower for 10KC10 than for 10KC8 or 6KC8 (Table 4). The rheological relaxation time is related to the average time required for a single chain end to be freed from the aggregate core in which it resides. For a chain to become completely free to leave the gel, both ends must be free, which would be a much rarer event, scaling as ~(viscoelastic time, τ_r)$^{-2}$. Release of a micelle from the gel might be even more rare.

Discussion

Comparison to Prior Studies of R_f-PEGs. This study represents the first report of sol−gel coexistence

in a fluorocarbon-terminated PEG system. However, in view of our results, it is surprising that previous studies of similar materials did not observe sol−gel phase separation. Menchen et al. reported the insolubility of 8KC8 in water, although it is not clear whether it precipitated or phase-separated.[15] Neither phase separation nor precipitation was reported for solutions of 6- or 10-kD PEG modified with $-C_{11}H_{22}C_8F_{17}$.[20,22] The origin of these discrepancies might lie in differences in chemical structure (the degree of end-capping) or in experimental methods (differences in methods have been implicated previously as the source of wide differences in the reported aggregation number for a given end group[17]). For example, the absence of any viscosity enhancement for a solution of 6-kD PEG modified with $-C_{11}H_{22}C_8F_{17}$[20] might have resulted from the low viscosity of the sol phase in which the coexisting gel might have been suspended. Also, the absence of phase separation in 10-kD PEG modified with $-C_{11}H_{22}C_8F_{17}$ might be due to the low conversion rate of end-capping (<80%).[36]

Implications for Biomedical Applications. For potential applications of bifunctional R_f-PEGs that demonstrate sol−gel coexistence as a delivery vehicle, it is desirable to have systematic control of gel properties such as composition and modulus, as well as transport properties such as diffusion coefficient and viscosity. The observed properties of the equilibrium gel phase of R_f-PEGs that exhibit sol−gel coexistence show that the gel composition, modulus, and viscosity can be adjusted by choice of the PEG midblock length, the end-group length, or both. The low concentration in the dilute phase translates into a small driving force for the dissolution of these gels when they are exposed to an open system (e.g., when used as an implant or as a drug-release depot). Also, the addition of salts causes a small increase in the equilibrium gel concentration and a decrease in the equilibrium sol concentration. The effect of dissolved salts (Table 3) will be present in vivo with the small, but beneficial, result of increasing the modulus and reducing the rate of dissolution.

By choice of the lengths of the hydrophilic PEG and hydrophobic end groups, the type and rate of erosion of the hydrogel can be controlled as well. The dissolution characteristics in an open system correlate with the type of phase behavior of the polymer matrix: Sol−gel coexistence provides a constant polymer concentration during the erosion process (Figure 8c) in contrast to the continuous decrease in the polymer concentration of the whole matrix for single-phase systems (Figure 8a,b). The constant polymer concentration during erosion at sol−gel equilibrium implies that erosion occurs only at the surface, indicating that this hydrogel degrades heterogeneously and that a constant release rate of an embedded nondiffusible target material can be achieved. A strong dependence of the erosion rate on the end-group length suggests that the erosion for sol−gel coexisting species is controlled by end-group dissociation. The absolute values of the dissolution rates of sol−gel coexisting species are sufficiently slow that such species would be appropriate for applications as delivery depots in the body.

Implications for Theory. The key features to capture regarding systems that exhibit sol−gel coexistence are the compositions of the equilibrium phases and the transition from single-phase to sol−gel coexistence behavior. As mentioned above, two models have been

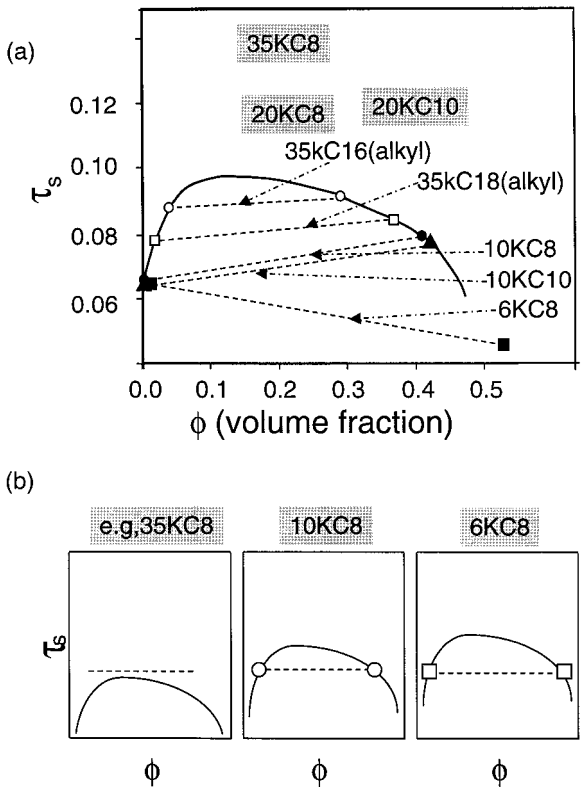

Figure 7. Phase diagram of the end-group-modified PEG systems (a) sticky hard-sphere phase diagram in terms of $\tau_s \sim$ (stickiness parameter)$^{-1}$, adapted from Figure 11 of ref 17; (b) possible explanation of the change in phase behavior with N in terms of a shift in the phase boundary as a result of changes in the intermicelle potential with PEG length (see text).

presented to capture the phase behavior of telechelic associating polymers: Semenov's scaling theory,[28] which describes how the aggregation number, p, and the number of segments of hydrophilic chain, N, affect the equilibrium gel concentration but cannot predict the quantitative composition of the equilibrium phases or the transition from single-phase to sol−gel coexistence behavior; and Pham et al.'s approach using the sticky hard-sphere model,[17] which makes quantitative predictions of the composition of the equilibrium phases and the transition from single-phase to sol−gel coexistence behavior but is formulated in terms of a stickiness parameter ($1/\tau_s$) that must be determined empirically to account for the experimental data. Here, we compare the observed phase behaviors of the present systems and those previously described in the literature to the predictions of each of these models, starting with the equilibrium gel concentration, then moving to the equilibrium sol concentration, and finally addressing the transition from single-phase to sol−gel coexistence behavior.

Equilibrium Gel Concentration. Experimental results show that the equilibrium gel concentration is more sensitive to PEG length ($\sim N$) than to the aggregation number (p, mainly determined by the end-group length[37,38]), in qualitative accord with the scaling relation predicted by Semenov, namely, $\phi^* \sim (p^{1/2}/N)^{3\upsilon-1}$, where ϕ^* is the average polymer concentration within the equilibrium gel and υ is the Flory exponent.[28] For example, pairwise comparisons for similar relative changes in p vs N in Pham et al.[17] show that increasing p from ~20 (35-kD PEG with C16 alkyl ends) to ~33

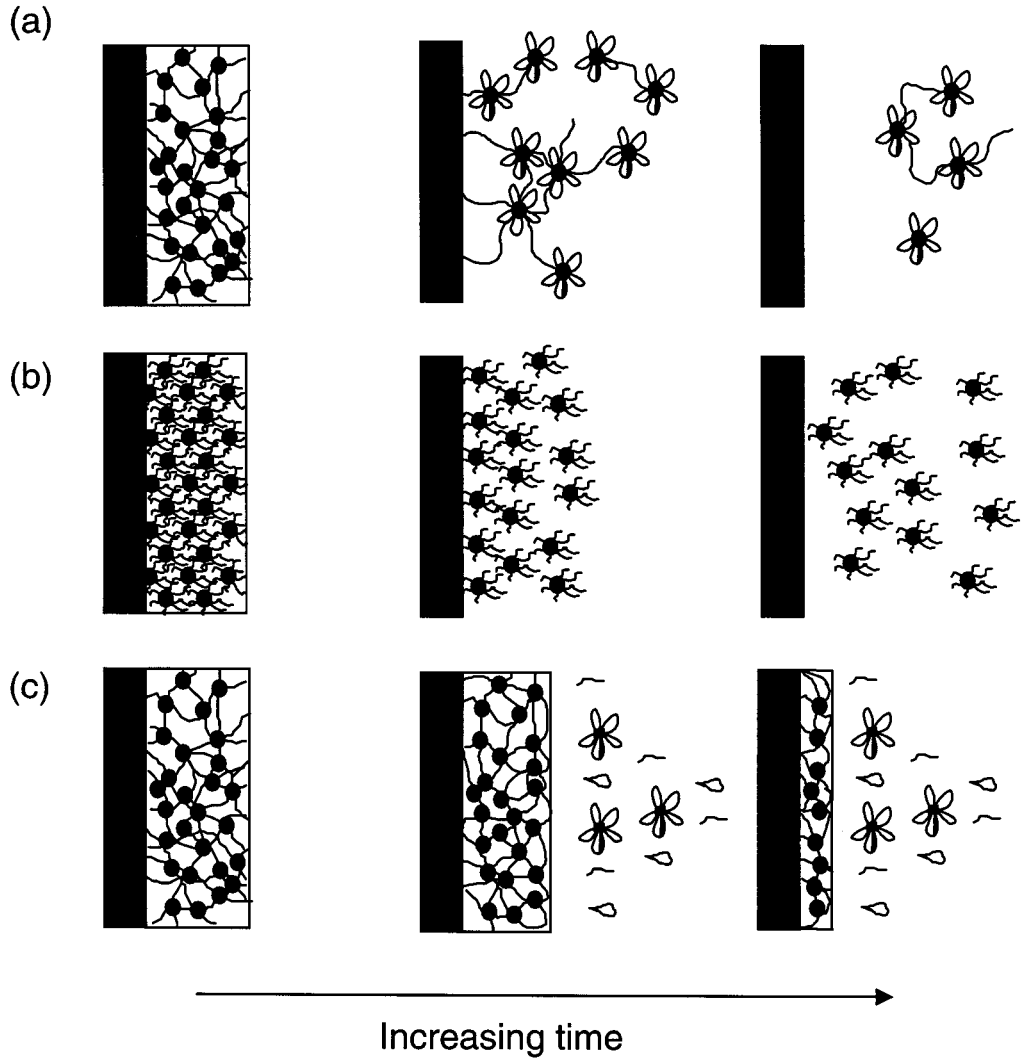

Figure 8. Schematic representation of dissolution of the polymer gel in an open environment: (a) single-phase species (e.g., 20KC10), (b) lyotropic cubic-phase gel (e.g., 5K−M−C10), (c) sol−gel coexisting species.

(35-kD PEG with C18 alkyl ends) gives a ∼17% increase in $C_{gel,eq}$ (Figure 8 of ref 17), whereas a decrease in PEG length from 35- to 20-kD PEG (both with C16 alkyl ends) gives a ∼65% increase in $C_{gel,eq}$ (Figure 8 of ref 17). From the present study, a ∼50% increase in p from 10KC8 to 10KC10, as determined by SANS,[38] gives no distinct change in $C_{gel,eq}$, whereas a ∼40% decrease in PEG length from 10KC8 to 6KC8 gives a ∼70% increase in $C_{gel,eq}$. Indeed, the observed behavior suggests that the greater sensitivity of $C_{gel,eq}$ to N than to p is even more pronounced than indicated by the Semenov scaling expression.

In the context of the model of Pham et al., the N dependence of the polymer concentration in the equilibrium gel arises solely from the decrease in polymer concentration within a micelle as N increases.[17] However, this does not fully account for the observed decrease in $C_{gel,eq}$ with increasing N.[40] The present fluoroalkyl-ended systems also illustrate the significant dependence of the intermicelle attraction on the PEG midblock length. The small difference in gel volume fraction between 10KC8 and 10KC10 (ϕ = ∼0.61 and ∼0.59, respectively)[41] suggests a weak dependence of the intermicelle attraction on p, while the significant difference between 10KC8 and 6KC8 (ϕ = ∼0.59 and ∼0.70, respectively)[41] shows a strong dependence on N (Figure 7a). This argues that the attraction between the micelles depends significantly on both p and N. In addition, the observed micellar volume fraction, ϕ, of the 6KC8 equilibrium gel is too large to describe using the adhesive hard-sphere phase diagram (Figure 7),[17] presumably because, unlike hard spheres, micelles can deform and even overlap.

Equilibrium Sol Concentration. The dependence of the equilibrium sol concentration on N and p reinforces the conclusion that the intermicelle attraction depends on both p and N. The most striking indication of this is the fact that the $C_{sol,eq}$ values for the present systems are much smaller than for those studied by Pham et al.[17] To account for $C_{sol,eq}$ being from 2 to 10 times lower, the intermicelle attraction would have to be substantially larger. In their application of the sticky hard-sphere model, this difference in intermicelle attraction would be attributed to a difference in p. However, there is very little change in intermicelle attraction with p,[38] and the aggregation numbers for the present fluroalkyl-ended systems are similar to those of the alkyl-ended PEG molecules of Pham et al.[39] Therefore, it is difficult to explain the smaller $C_{sol,eq}$ values on the basis of p alone. On the other hand, the present systems show very large changes in phase behavior with PEG length (Table 3). Therefore, we believe that the low values of $C_{sol,eq}$ in the present systems might predominantly reflect the shorter PEG lengths in this study (which were 10- and

6-kD PEG) compared to those in Pham et al. (which were 20- and 35-kD PEG).

The relative values of the equilibrium sol and gel volume fractions[41] also support the need to incorporate physical interactions not included in the sticky hard-sphere model. For one system (35-kD PEG with C16 alkyl ends), Pham et al. found good agreement among the values of the stickiness parameter (τ_s^{-1}) inferred from three different characteristics: the second virial coefficient (from dynamic light scattering at $C < C_{sol,eq}$), $\phi_{sol,eq}$, and $\phi_{gel,eq}$. However, for 35-kD PEG with C18 alkyl ends, the τ_s value inferred from light scattering ($\tau_s \approx 0.07$) was substantially lower than the two different values of τ_s inferred from $\phi_{sol,eq}$ and $\phi_{gel,eq}$[17] (Figure 7a). The discrepancies between the values of τ_s inferred from $\phi_{sol,eq}$ and $\phi_{gel,eq}$ are even more pronounced in our systems (10KC10, 10KC8, and 6KC8 in Figure 7a).[42] Indeed, for 6KC8, $\phi_{gel,eq}$ is simply too large to be explained within the context of the sticky hard-sphere model (Figure 7a).

Transition from Single-Phase to Sol−Gel Coexistence Behavior. Three fluoroalkyl-terminated PEGs exhibiting single-phase behavior have been described that are particularly instructive to compare to the systems that exhibit sol−gel equilibrium, namely, the 35KC8 system studied by Winnik and co-workers[14,15] and the 20KC10 and 20KC8 systems of the present study. All of these systems show that PEG length plays a very large role, as pairwise comparisons can be made to systems with the same hydrophobe (35KC8 and 20KC8 vs 10KC8, and 20KC10 vs 10KC10). Considering the insensitivity of the intermicelle attraction to p,[17] the change in phase behavior as the PEG is increased from 10 to 20 kD (Figure 7a) also indicates that the intermicelle attraction is very sensitive to N.

Regarding the effect of end group at fixed N and similar p, for 35-kD PEG, Winnik et al. found that 35KC8 showed single-phase behavior, whereas Pham et al. found that 35-kD PEG with C16 or C18 alkyl ends showed sol−gel coexistence. If the aggregation number for 35KC8 is indeed similar to that for 10KC8 ($p \approx 30$[39]), it is larger than that for the 35-kD PEG with C16 alkyl groups and similar to that for 35-kD PEG with C18 alkyl ends.[17] Therefore, one would expect 35KC8 to have intermicelle attraction as strong as that for 35-kD PEG with C18 alkyl ends and to exhibit sol−gel coexistence (Figure 7a), which is not the case. Similarly, a comparison of 20KC10 to 20-kD PEG with C16 alkyl ends shows the surprising result that 20KC10 exhibits single-phase behavior even though it has a larger p ($\sim$50[39]) than 20-kD PEG with C16 alkyl ends ($p \approx 20$, based on 35kD PEG with C16), which exhibits sol−gel coexistence.

These comparisons show effects of p for fixed PEG length that are contrary to the physics of both the Semenov model and the model of Pham et al. This discrepancy suggests that the type of hydrophobe plays an important role that is not captured by current models (fluoroalkyl-ended systems show weaker intermicelle attraction than their alkyl ended couterparts). Perhaps this reflects a difference in corona structure resulting from the difference in core structure. It is believed that fluoroalkyl groups behave as short rods that aggregate laterally such that the PEG chains must emerge from the faces of the fluoroalkyl aggregate core, whereas alkyl groups form liquidlike, spherical cores that do not as tightly constrain the lateral spacing of the PEG chains.

Unexplained Effects of N and Hydrophobe Type. Current physical models of the interactions between micelles lead to interaction potentials that are independent of N because the softer repulsion with increasing N is offset by the increasing area over which the repulsion acts when micelles come into contact, which is valid whether the chains in the corona are stretched or not.[17,28,43] Consequently, the intermicelle interaction potential used by both Semenov and Pham et al. is determined exclusively by the aggregation number of the hydrophobic core. In contrast, the phase behaviors of the present systems, 20KC10 vs 10KC10 and 10KC8 vs 6KC8, and the previously reported data[14,15,17] consistently reveal that the intermicelle interaction potential is also affected by the size of the micelle (determined by the PEG midblock length).

The substantial effect of PEG length on phase behavior could qualitatively be explained by a change in shape of the intermicelle interaction potential. It is known that small changes in interparticle potential $\Phi(r)$ can cause profound shifts in the phase boundary.[44,45] In the context of micelles, a change in $\Phi(r)$ might result from a crossover from having strong chain stretching to weak chain stretching as N increases. Such a change would be reasonable, given that the outermost blob size, ξ_o, was half the micelle radius R for 35-kD PEG with C18 alkyl ends ($p \approx 30$),[17] indicating that this relatively long PEG was not substantially stretched. However, as the PEG length decreases, ξ_o/R is expected to decrease in the crossover regime between unstretched and stretched brushes, making the intermicelle potential steeper. Thus, the observed phase behavior might indicate that, for an approximately fixed aggregation number (set by the hydrophobe), the change in the character of the corona (e.g., degree of stretching) might cause the position of the gas−liquid phase boundary to shift (Figure 7b).

The peculiarities in the phase behavior of PEG itself might cause one to question whether the explanation of the observed N dependence could be PEG-specific. For example, PEG displays an unusual dependence of solvent quality on PEG concentration. Increasing the PEG concentration produces significantly poorer solvent conditions.[46] Accordingly, with increasing molecular weight of the PEG, and thus increasing blob size for the outermost corona, the solvent quality improves. Therefore, bringing micelles together for larger PEG midblocks might cost more free energy (by increasing the PEG−PEG contacts when the outer corona is in a good solvent condition) than bringing micelles together for shorter PEG midblocks (because they were in a poorer solvent condition, so having increased PEG−PEG contacts costs less). However, in the concentration range relevant here ("outer blob" concentrations of 2−6 wt %), this effect seems to be too small to explain the large change in the interaction potential suggested by the observed phase behavior.[46,47]

In search of some physical explanation for the observed effects of hydrophobe type and PEG length on the position and nature of the sol−gel coexistence curve and the character of the resulting gels, one could consider the interfacial energy of the hydrophobic core and how its effect is progressively shielded with increasing N. One might speculate that increasing PEG length might screen the hydrophobic core more effectively, so the micelle would be more soluble (weaker intermicelle attraction). However, because the PEG

chains are stretched near the cores of all of the micelles reported in the literature, it seems that the identity of the core would be well shielded in all existing systems. Therefore, we do not know how important this effect would be. Thus, understanding the observed effects of PEG length and hydrophobe type appears to be an unsolved problem.

Conclusions

The phase behavior, rheology, and erosion kinetics of bifunctional R_f-PEGs provide a unified picture and show that the material properties of this class of hydrogels can be systematically tuned over a wide range. By judicious choice of the lengths of the PEG and fluoroalkyl end groups, different phase behaviors—from single-phase behavior, to sol−gel coexistence (phase separation), to essentially insoluble precipitation—are obtained. For polymers that exhibit sol−gel coexistence, the swelling ratio and modulus of the gel phase are determined by the PEG midblock length, the relaxation time and erosion kinetics are dominated by the hydrophobe length, and the viscosity and equilibrium sol concentration depend on both PEG midblock and hydrophobe length.

The accessibility of sol−gel coexistence behavior has a number of important implications for potential applications of PEG hydrogels formed by aggregation of hydrophobes. By providing hydrogels that exhibit surface erosion at low enough rates to be useful, these materials are candidates for applications in the controlled release of therapeutic proteins and in tissue engineering. A quantitative theoretical description of the phase behavior remains elusive, particularly the effects of the PEG length, the hydrophobe type, and the soft (deformable and compressible) nature of micelles.

Acknowledgment. This research was supported in part by a grant from NSF (CTS-9729443), a graduate fellowship from the Korean Ministry of Education (GT), and by the MRSEC Program of NSF (DMR-0080065).

References and Notes

(1) Deluca, P. P.; Mehta, R. C.; Hausberger, A. G.; Thanoo, B. C. In *Polymeric Delivery Systems*; American Chemical Society: Washington, D.C., 1993; pp 53−79.
(2) Holland, S. J.; Tighe, B. J.; Gould, P. L. *J. Controlled Release* **1986**, *4*, 155.
(3) Sawhney, A. S.; Hubbell, J. A. *J. Biomed. Mater. Res.* **1990**, *24*, 1397.
(4) Domb, A. J.; Gallardo, C. F.; Langer, R. *Macromolecules* **1989**, *22*, 3200.
(5) Heller, J.; Perhale, D. W. H.; Helwing, R. F.; Fritzinger, B. K. *Polym. Eng. Sci.* **1981**, *21*, 727.
(6) Sawhney, A. S.; Pathak, C. P.; Hubbell, J. A. *Macromolecules* **1993**, *26*, 581.
(7) Sawhney, A. S.; Pathak, C. P.; van Rensburg, J. J.; Dunn, R. C.; Hubbell, J. A. *J. Biomed. Mater. Res.* **1994**, *28*, 831.
(8) Zaho, X.; Harris, J. M. *J. Pharm. Sci.* **1998**, *87*, 1450.
(9) Harris, J. M. *Poly(ethylene glycol) Chemistry. Biotechnical and Niomedical Applications*; Plenum Press: New York, 1992.
(10) Han, D. K.; Hubbell, J. A. *Macromolecules* **1996**, *29*, 5233.
(11) West, J. L.; Hubbell, J. A. *Macromolecules* **1999**, *32*, 241.
(12) Rubinstein, M.; Dobrynin, A. V. *Trends Polym. Sci.* **1997**, *5* (6), 181.
(13) Annable, T.; Buscall, R.; Ettelaie, R. *J. Rheol.* **1993**, *37* (4), 695.
(14) Menchen, S.; Johnson, B.; Winnik, M. A.; Xu, B. *Chem. Mater.* **1996**, *8*, 2205.
(15) Menchen, S.; Johnson, B.; Winnik, M. A.; Xu, B. *Electrophoresis* **1996**, *17*, 1451.
(16) Pham, Q. T.; Russel, W. B.; Lau, W. *J. Rheol.* **1998**, *42* (1), 159.
(17) Pham, Q. T.; Russel, W. B.; Thibeault, J. C.; Lau, W. *Macromolecules* **1999**, *32* (9), 2996.
(18) Pham, Q. T.; Russel, W. B.; Thibeault, J. C.; Lau, W. *Macromolecules* **1999**, *32* (15), 5139.
(19) Francois, J.; Maitre, S.; Rawiso, M.; Sarazin, D.; Beinert, G.; Isel, F. *Colloids Surf. A* **1996**, *112*, 251.
(20) Xu, B.; Li, L.; Yekta, A.; Masoumi, A.; Kanagalingam, S.; Winnik, M. A.; Zhang, K.; Macdonald, P. M.; Menchen, S. *Langmuir* **1997**, *13* (9), 2447.
(21) Cathebras, N.; Collet, A.; Viguier, M.; Berret, J *Macromolecules* **1998**, *31*, 1305.
(22) Serero, Y.; Aznar, R.; Porte, G.; Berret, J.-F.; Calvet, D.; Collet, A.; Viguier, M. *Phys. Rev. Lett.* **1998**, *81* (25), 56584.
(23) Jenkins, R. D.; Silebi, C. A.; El-Asser, M. A. *Polym. Mater. Sci. Eng.* **1989**, 629.
(24) Kaczmarski, J. P.; Glass, J. E. *Macromolecules* **1993**, *26*, 5149.
(25) Lundberg, D. J.; Brown, R. G.; Glass, J. E.; Eley, R. R. *Langmuir* **1994**, *10*, 3027.
(26) Tam, K. C.; Jenkins, R. D.; Winnik, M. A.; Bassett, D. R. *Macromolecules* **1998**, *31*, 4149.
(27) de Gennes, P. G. *Scaling Concepts in Polymer Physics*; Cornell University Press: Ithaca, NY, 1979.
(28) Semenov, A. N.; Joanny, J. F.; Khokhlove, A. R. *Macromolecules* **1995**, *28*, 1066.
(29) Zhang, H.; Pan, J.; Hogen-Esch, T. E. *Macromolecules* **1998**, *31*, 2815.
(30) Childs, C. E. *Microchem. J.* **1975**, *20*, 190.
(31) Aust, E. F.; Ito, S.; Sawodny, M.; Knoll, W. *Trends Polym. Sci.* **1994**, *2* (9), 313.
(32) Bailey, F. E., Jr; Callard, R. W. *J. Appl. Polym. Sci.* **1959**, *1* (1), 56.
(33) To examine carefully whether 10KC8 and 6KC8 also follow the single-relaxation behavior, we need to obtain the data in the frequency window above the crossover frequency, ω_x. Unfortunately, in the accessible range of frequency (up to 100 rad/s), we cannot go much beyond ω_x for C8 fluoroalkyl-ended PEGs.
(34) (a)Vrentas, J. S.; Duda, J. L.; Hou, A.-C. *J. Appl. Polym. Sci.* **1984**, *29*, 399. (b) Scranton, A. B.; Klier, J.; Peppas, N. A. *Polymer* **1990**, *31*, 1288. (c) Franson, N. M.; Peppas, N. A. *J. Appl. Polym. Sci.* **1983**, *28*, 1299. (d) Titow, W. V.; Braden, M.; Currell, B. R.; Loneragan, R. J. *J. Appl. Polym. Sci.* **1974**, 1*8*, 867. (e) Kim, D.; Caruthers, J. M.; Peppas, N. A. *Macromolecules* **1993**, *26*, 1841.
(35) Jeong, B.; Bae, Y. H.; Lee, D. S.; Kim, S. W. *Nature* **1997**, *338*, 860.
(36) Berret, J.-F. University of Montpellier II, Montpellier, France. Private communication.
(37) Alami, E.: Almgren, M.; Brown, W.; Francois, J. *Macromolecules* **1996**, *29*, 2229.
(38) The weak effect of τ_s is evident first in the relatively small decrease in τ_s from ∼0.091 to ∼0.067 as p increases from ∼20 to ∼33[17] and second in the small change in $C_{sol,eq}$ as p increases from ∼30 (10KC8) to ∼30 (10KC8); see Table 3.[39]
(39) Tae, G.; Kornfield, J. A.; Hubbell, J. A.; Lal, J., manuscript in preparation. From SANS, we observed that the aggregation number is dominated by the end-group length: both 20KC10 and 10KC10 have $p \approx 50$, and both 10KC8 and 6KC8 have $p \approx 30$.
(40) It is challenging to make quantitative comparisons to the predicted phase behavior. First, from measured mass concentrations, one must compute the corresponding volume fraction; however, the uncertainty in the determination of the micelle volume is large, particularly when using $[\eta]$ for PEG at 25 °C.[41] Next, an independent determination of the stickiness parameter from dynamic light scattering can be applied only to polymers of high enough solubility and has substantial uncertainty. In evaluating the relative change in $C_{gel.,eq}$ reported in Figure 8 of ref 17 as the PEG length increased from 20 to 35 kD, if one uses the reported insensitivity of τ to p,[17] the insensitivity of p to PEG length for fixed hydrophobe,[38] and the reported effect of PEG length on $[\eta]$,[41] it is only possible to explain approximately two-thirds of the observed change in $C_{gel.,eq}$. However, considering the sensitivity of equilibrium sol and gel volume fractions to the stickiness parameter in the sticky hard-sphere phase diagram and the uncertainties in experimental determinations of the stickiness parameter from light scattering and of the mass/volume of micelles from intrinsic viscosity, it is difficult to make a quantitative evaluation.

(41) The volume fractions were estimated using $[\eta]c/2.5$ as used in ref 17. The $[\eta]$ values were estimated using the relation for pure PEG of $[\eta] = 4.33 \times 10^{-4} \times (M_w)^{0.679}$ (dL/g) (Kawaguchi et al. *Polymer* **1997**, *38*, 2885), based on the result that there is no noticeable difference between the $[\eta]$ values of hydrophobically modified PEG and unmodified PEG in ref 17. However, there are a number of caveats regarding this method. First, $[\eta]$ is the volume per mass at infinite dilution, but significant overlap among micelles is postulated when they are phase-separated; the outermost blob size (anticipated overlap width) was about one-half the radius of the micelle for the systems in ref 17. Second, there are various ranges of reported $[\eta]$ values for PEG, as discussed in ref 17. Considering the sensitivity of the inferred stickness parameter to the volume fractions of the equilibrium sol and gel in the sticky hard-sphere phase diagram, a small change in $[\eta]$ will cause the significant change in the stickness parameter inferred from the measured mass fractions of each phase.
(42) An estimation of stickiness parameters was not possible for our system because of the very low $C_{sol,eq}$ values.
(43) Daoud, M.; Cotton, J. P. *J. Phys.* **1982**, *43*, 531.
(44) Hagen, M. H. J.; Frenkek, D. *J. Chem. Phys.* **1994**, *101*, 4093.
(45) Bellier-Castella, L., Xu, H., Baus, M. *J. Chem. Phys.* **2000**, *113*, 8837.
(46) Bae, Y. C.; Shim, J. J.; Soane, D. S.; Prausnitz, J. M. *J. Appl. Polym. Sci.* **1993**, *47*, 1193.
(47) Venohr, H.; Fraaije, V.; Strunk, H.; Borchard, W. *Eur. Polym. J.* **1998**, *34*, 723.

MA0107511